Anodic Dissolution of Cu-Zn-Ni Alloy Scraps in Copper(II) sulphate solution

Zuxuan Wu[1,2,3], Lei Li[1,2,3,], Jiayun Wang[2,3], Yu Wang[2,3]*

[1] State Key Laboratory of Complex Non-ferrous Metal Resources Clean Utilization, Kunming University of Science and Technology, Kunming 650093, China.
[2] Engineering Research Center of Metallurgical Energy Conservation and Emission Reduction of Ministry of Education, Kunming University of Science and Technology, Kunming 650093, China.
[3] Faculty of Metallurgical and Energy Engineering, Kunming University of Science and Technology, Kunming 650093, China.
*E-mail: tianxiametal1008@163.com

In this work, the anodic dissolution properties of Cu-Zn-Ni alloy scraps in 45 g L^{-1} $CuSO_4$ solutions have been analyzed. The analysis methods employed were potentiodynamic polarization techniques, electrochemical impedance spectroscopy and electron probe microscopic analysis. In a certain range, the anodic dissolution of the Cu-Zn-Ni alloy scraps in $CuSO_4$ solutions increased with the H_2SO_4 concentration and temperature. The overall dissolution of the Cu-Zn-Ni alloy scraps were found to be under anodic control; further, the anodic dissolution process was under diffusion control deduced from the activation energy of the anode dissolution process being 14.6 kJ mol^{-1}. After heat treating the alloy scraps, the Cu-Zn-Ni alloy scraps were found to be more susceptible to dissolution due to the increase of the size of the grains and the decrease of the particle size uniformity.

1. INTRODUCTION

Copper and its alloys have wide industrial applications due to their high technological value, including in marine environments, building materials, electric materials, and the mechanical industry. [1-4] Correspondingly, due the end of the service life of these copper-based alloys, there will be large amounts of copper-based alloy scraps that are produced. As a result of the depletion of natural copper resources, the recovery of copper from these copper-based scraps has been studied in recent years. [5-8]

Currently, copper-based alloy scraps are mainly treated and recycled by using pyrometallurgical or hydrometallurgical methods and the former is currently the dominant way in the industry. [9-11] The pyrometallurgical methods, such as processes of ISASMELT, Outokumpu, and Ausmelt smelting, mainly include the steps of smelting, fire-refining, and electrorefining. The advantages of these pyrometallurgical methods are their (1) low investment and operating costs, (2) high reaction rates and (3) reliable and proven processes and equipment. [12,13] However, many associated metals in the copper-based alloy scraps will enter the slag during the smelting process, thereby causing secondary losses. [14,15] The traditional hydrometallurgical treatment of these copper-based scraps, including the steps of leaching, extraction and electrowinning, is proposed as a low-cost technology. However, the drawbacks including high consumption of chemical reagents, secondary environmental pollution, and complex process flows make it difficult to be applied in industry. [16,17] It is noteworthy that, a direct electrolysis process has also been developed in which the copper-based alloy scraps are used as anode and the copper is selectively deposited at the cathode due to the potential difference between copper and other associated metals including Ni, Zn, Al, etc. [18] In Chile, the process of recovering copper from copper scraps with the copper scraps used as anode has been applied in industry. Meanwhile, the copper qualitatively free from impurities could also be obtained from printed circuit board wastes through the similar process. [19-21] Also through a direct electrolysis process, a copper with purity of 99.98 wt% was produced from the anodes of Cu-based alloy scraps [22].

The anodic dissolution is important for this direct electrolysis process to be carried out effectively. The anodic dissolution of copper or copper-based alloys in various electrolytes has been widely investigated. In chloride-sulfate electrolytes, Waheed A. Badawy et al. [23] found that passivation would occur once a protective barrier oxide film (Al_2O_3 and Cu_2O) was formed on the anode surface during the dissolution of Cu-10Al-5Ni alloy. With respect to the electrochemical behavior of Cu-Zn alloy in a chloride solution, John W. Bond OBE and Elaine Lieu [24] found that a passivating layer consisting of ZnO could also be formed after a period of 24 h when the NaCl concentration was below 0.2 M. While in the initial stages, Zn had little effect on the copper dissolution in the sulfate solution and the corrosion current density increased as the Zn content increased, which might be due to the preferential corrosion of Zn. To decrease the passivation, Mohammed A. Amin et al. [25] found that decreasing the solution's pH or increasing the temperature was conducive to the copper anode's dissolution. Heat treatment also plays an essential role in decreasing the passivation through altering the grain size and secondary phase volume fraction in the sample. [26-30] Y. Lu et al. found that the Mg–Zn–Ca alloy with the smallest grain size but the largest secondary phase volume fraction was the most susceptible to dissolution in simulated body fluid at 37 °C. [26]

A direct electrolysis process for recovering Cu from Cu-Zn-Ni alloy scraps was used in our research. In the present work, the anodic dissolution behavior of Cu-Zn-Ni alloy scraps in $CuSO_4$ electrolytes was studied under different conditions of sulfuric acid concentration, potential scan rate, temperature and heat treatment. Various electrochemical techniques, e.g., potentiodynamic polarization, cyclic voltammetry and electrochemical impedance spectroscopy (EIS), were used.

2. EXPERIMENTAL SECTION

2.1 Specimen preparation

The materials used in this research were Cu-Zn-Ni alloy scraps from a mechanical industry. The mass contents of the Cu-Zn-Ni alloy scraps were given in Table 1. 1-mm-thick sheets were produced from these Cu-Zn-Ni alloy scraps. Then, the Cu-Zn-Ni alloy sheets were heat treated in three different forms, viz. as-cast, A (heated up to 200 °C and then held for 20 h and water quenched) and B (heated up to 500 °C and then held for 20 h and water quenched).

Table 1. Inductively coupled plasma mass spectrometry of the Cu-Zn-Ni alloy scrap

Element	Cu	Zn	Ni	Fe	Mn	Si	Pb
Percentage (%)	61	30.5	7.9	0.2	0.06	0.3	0.06

2.2 Experiment

All experiments were carried out in 300 mL test solutions prepared with analytical grade chemical reagents and deionized water, and $CuSO_4$ concentration of 45 g L^{-1} in the solutions was used as the base. The specimens were clamped using an electrode holder and sealed using epoxy resin leaving a surface area of 0.25 cm^2, which was used as the working electrode. A stainless steel sheet (Austenitic grade 316) with an area of 8 cm^2 was used as an auxiliary electrode and a saturated calomel electrode (SCE) was employed as the reference electrode to which all potentials are referred. Before each experiment, the surface of the working electrode was polished with different grades of emery papers up to 2000 grit, rinsed with acetone and distilled water, and then transferred quickly to the electrolytic cell.

The electrochemical measurement studies were carried out using an electrochemical workstation (RARSTAT2273) and a personal computer. The potentiodynamic curves were recorded at the potential ranging from -0.35 V to 0.4 V setting the potential scan rate of 5 mV s^{-1}. The scan rate of the linear sweep voltammograms was 5 mV s^{-1}, and the sweeping region is from -0.5 V to 6.5 V. Cyclic voltammetric measurements were conducted by linearly sweeping the potential from -0.6 V to 2.0 V at a proper scan rate. The electrochemical impedance investigations were measured in the frequency range of 0.1 to 10^5 Hz with alternating current amplitude of 5 mV at an open-circuit potential. Each test was conducted in an aerated stagnant solution at the required temperature (±1 °C) using a water thermostat for at least three times to achieve reproducibility.

2.3 Characterization

The chemical composition of the Cu-Zn-Ni alloy scraps was characterized by chemical analysis. The X-ray diffraction (Rigaku D/max-3B) test was used to analyze the phase components of the specimens. The tested samples were polished to a scratch-free surface and then etched in a corrosive

substance before the electron probe microanalysis (EPMA-JAX8230, JEOL, Japan) was used to detect the microstructure of them.

3. RESULTS AND DISCUSSION

3.1 Effect of H₂SO₄ concentration on the Cu-Zn-Ni alloy scraps anodic dissolution

3.1.1 Potentiodynamic polarization curves

Fig. 1 shows the potentiodynamic polarization that was recorded for the tested samples in 45 g L^{-1} CuSO₄ solutions in the absence and presence of various concentrations of H₂SO₄ [0-160 g L^{-1}] at a scan rate of 5 mV s^{-1} at 25 °C. The anode branch of the Tafel plots shows the Cu-Zn-Ni alloy scraps' dissolution, and the cathodic one represents the copper ions' reduction. Generally, the formation of Cu$^+$ is carried out simultaneously with the dissolution of the alloy scraps in the test solution, and then it will be further oxidized to Cu^{2+} ion. The dissolution reaction of the Cu-Zn-Ni alloy scraps in the test solutions can be described as follow: [23,31]

$$(aCu + bZn + cNi) + 0.5\,(a + b + c)\,O_2 + 2\,(a + b + c)\,H^+ \rightarrow$$
$$aCu^{2+} + bZn^{2+} + cNi^{2+} + (a + b + c)\,H_2O \qquad [1]$$
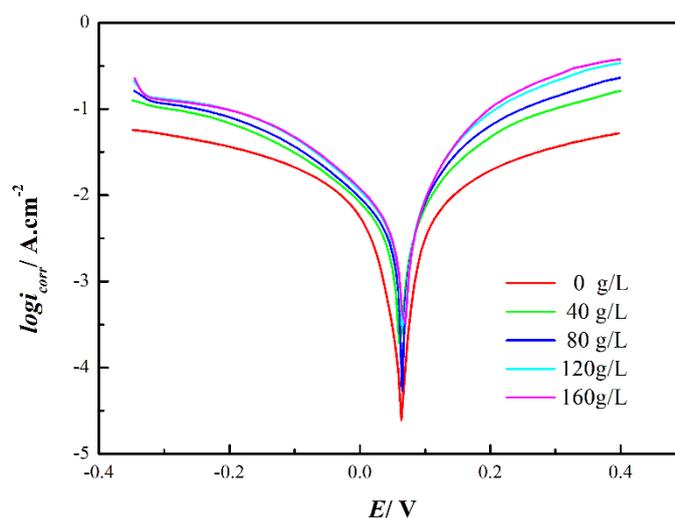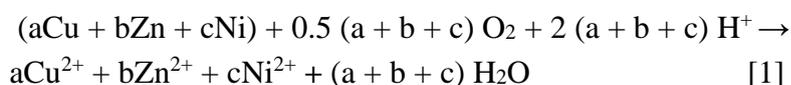
Figure 1. Potentiodynamic polarization curves for Cu-Zn-Ni alloy scraps in 45 g L^{-1} CuSO₄ solutions as a function of H₂SO₄ concentration at scan rate 5 mV s^{-1} at 25±1 °C

The values of the corrosion current density i_{corr}, the corrosion potential E_{corr}, the anodic Tafel slope β_a and cathodic Tafel slope β_c were calculated and summarized in Table 2. It is noted that the cathodic Tafel slopes are greater than the respective anodic Tafel slopes in Table 2. Then the conclusion can be drawn that the overall dissolution process kinetics of the Cu-Zn-Ni alloy scraps in the text solutions are under anodic control. [32,33]

Table 2. Corrosion parameters of the Cu-Zn-Ni alloy scraps in 45 g L^{-1} CuSO$_4$ solutions containing different H$_2$SO$_4$ concentration at 25±1°C

[H$_2$SO$_4$]/g L^{-1}	β_a/mV decade^{-1}	β_c/ mV decade^{-1}	i_{corr}/A	E_{corr}/V
0	136	158	6.231×10^{-4}	0.051
40	134	159	1.034×10^{-3}	0.050
80	129	152	1.186×10^{-3}	0.046
120	114	149	1.311×10^{-3}	0.051
160	117	127	1.554×10^{-3}	0.046

As the sulfate ions increase, more adsorbed species will be formed, as shown in Eqs. (2)-(4). Then, they dissolve into the solution and transform to CuSO$_{4aqs}$, ZnSO$_{4aqs}$ and NiSO$_{4aqs}$, which leads to corrosion of the Cu-Zn-Ni alloy scraps. [25] It is clearly shown in Table II that the i_{corr} increases from 6.231×10^{-4} to 1.554×10^{-3} A cm^{-2} with H$_2$SO$_4$ concentration from 0 to 160 g L^{-1}.

$$Cu + SO_4^{2-} = Cu(SO_{4aqs})^{2-} \qquad [2]$$
$$Zn + SO_4^{2-} = Zn(SO_{4aqs})^{2-} \qquad [3]$$
$$Ni + SO_4^{2-} = Ni(SO_{4aqs})^{2-} \qquad [4]$$
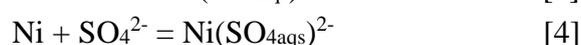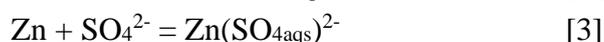
3.1.2 Potentiodynamic anode polarization curves

The potentiodynamic anodic polarization results of the Cu-Zn-Ni alloy scraps in the test solution with different H$_2$SO$_4$ concentrations are shown in Fig. 2. These curves exhibit a well-defined anodic peak (ABC) and then a passive region (CD) and at last an unexpected increase in the anode current (DE).
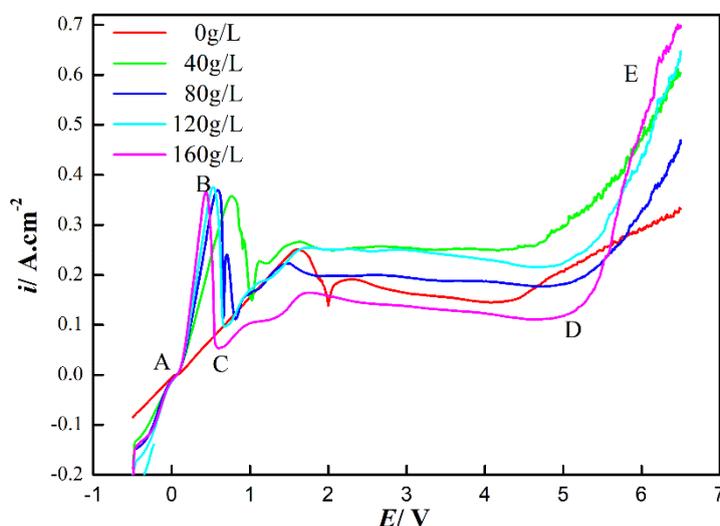
Figure 2. Potentiodynamic anode polarization curves for Cu-Zn-Ni alloy scraps in 45 g L^{-1} CuSO$_4$ solutions as a function of sulfuric acid concentration at scan rate 5 mV s^{-1} at 25±1 °C

The anodic peak consists of two parts: the active region (AB) and active-passive transition region (BC). The active region corresponds to the dissolution process of the Cu-Zn-Ni alloy scraps, in which the copper, zinc and nickel ions are dissolved in the electrolyte. The active-passive transition region represents the transitional period from the dissolution to passivation. During it, the passivation products formed might be oxides of Cu_2O, NiO and ZnO seen from Fig.3. [34] With these oxides being a solid electrolyte, an electrochemical double layer should be established at the oxide-solution interface. At this interface, oxygen ions are taken up in the oxides. The oxygen ions could be formed according to Eqs. (5)-(7). The generated copper, zinc and nickel ions egress and the O_{ads}^{2-} ions ingress across the oxide film under a high electric field. These processes bring about the formation of an oxide film on the anode surface, indicating the onset of passivation. [25,35]

$$H_2O = OH_{ads}^- + H^+ \qquad\qquad [5]$$
$$OH_{ads}^- = O_{ads}^{2-} + H^+ \qquad\qquad [6]$$
$$O_{ads}^{2-} = O_{ox}^{2-} \qquad\qquad\qquad [7]$$

This protective barrier oxide film formed on the alloy scrap surface separates the alloy scraps from the electrolyte and causes the occurring of the passive region (CD).

The region corresponding to the anodic current abruptly increasing is called the trans-passive region (DE), in which the passive layer is destructed attributed to the electrochemical (Reaction 8) and/or chemical oxidation of Cu_2O (Reaction 9) to more soluble CuO in the acidic solution after arriving at a certain potential. [36]

$$Cu_2O \rightarrow Cu^{2+} + CuO + 2e^- \qquad\qquad [8]$$
$$Cu_2O + 1/2O_2 \rightarrow 2CuO \qquad\qquad [9]$$
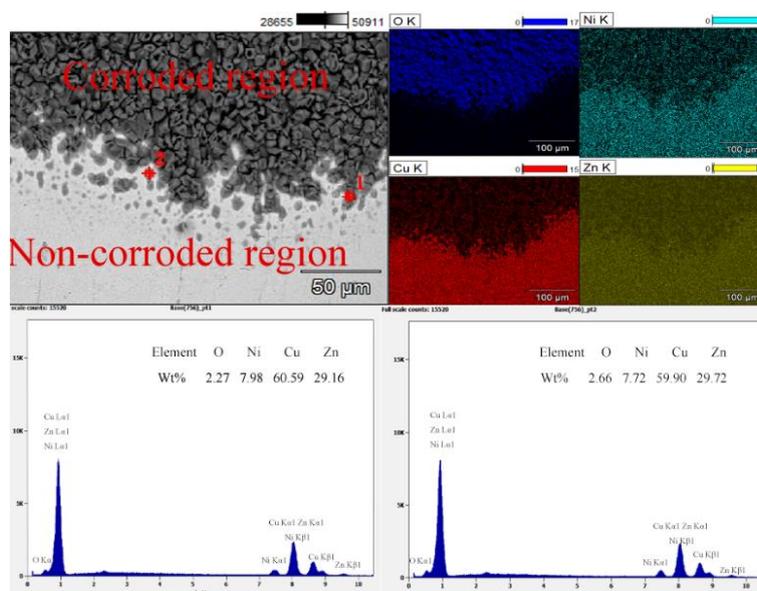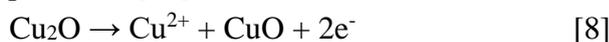
Figure 3. SEM mappings and SEM-EDS analysis of the Cu-Zn-Ni alloy scraps in 45 g L^{-1} CuSO$_4$ solutions containing 160 g L^{-1} H$_2$SO$_4$ at passive region at 25±1 °C

Fig. 2 shows that the anodic peak potentials become more negative and the slopes of the active region increase as the H_2SO_4 concentration increases from 40 to 160 g L^{-1}, which indicates that the alloy scraps are dissoved faster as the H_2SO_4 concentration increase. It is noteworthy that, the potential value E_b, which represents the breakdown potential of the passive layer, shifts towards more positive values in the test solutions with H_2SO_4 concentrations increasing from 0 to 160 g L^{-1} seen from Fig. 2. This is attributed to the dezincification of the Cu-Zn-Ni alloy scraps in the aqueous solution. The dezincification corrosion has two forms: pit wise and layer wise. The former occurs in a local area of the alloy scraps surface, while the latter occurs over the entire surface which causes the E_b increases. In general, pit dezincification occurs in neutral or weakly acidic electrolytes, and layer dezincification occurs in acidic electrolytes. [37]

3.2 Effect of potential scan rate and temperature on the Cu-Zn-Ni alloy scraps anodic dissolution

3.2.1 Effect of potential scan rate

The effect of the potential scan rate, v (5-100 mV s^{-1}), on the cyclic polarization curves of the Cu-Zn-Ni alloy scraps was studied, and the result is shown in Fig. 4. As observed in Fig. 4 (a), the anode peak current density (i_{pa}), anode peak potential (E_{pa}) and anode half-peak potential ($E_{pa/2}$) increase with the potential scan rate. The i_{pa} that were derived from the cyclic polarization curves obtained at different scan rates and the square root of the scan rate ($v^{1/2}$) have a good linear correlation, thereby indicating that the dissolution of the Cu-Zn-Ni alloy scraps in the test solutions are controlled by diffusion. [38,39]
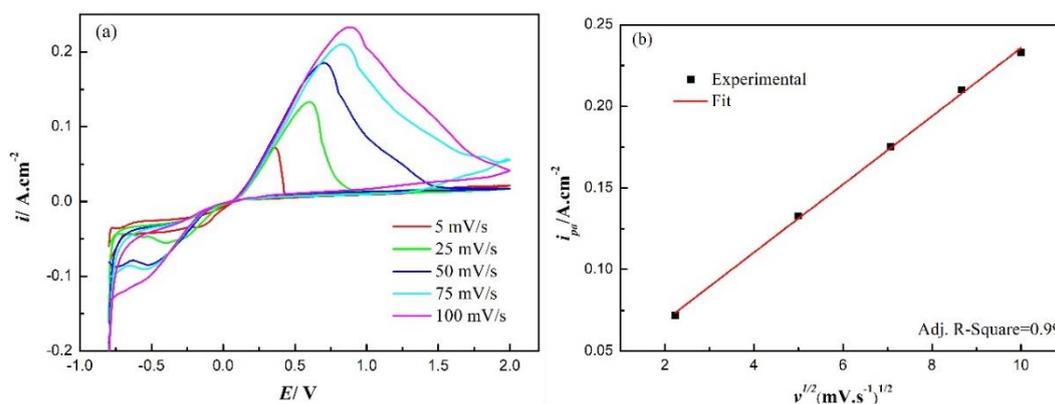
Figure 4. Cyclic polarization plots recorded for Cu-Zn-Ni alloy scraps in 45 g L^{-1} $CuSO_4$ solutions containing 160 g L^{-1} H_2SO_4 with various scan rates at 25± 1 °C: (a) Effect of potential scan rate on cyclic polarization curves; (b) Linear correlation of the anode peak current density against the square root of scan rate

3.2.2 Effect of temperature

The effect of temperature ranging from 25 °C to 60 °C on the corrosion of the Cu-Zn-Ni alloy scraps was researched. From the potentiodynamic polarization data obtained at the steady state, these

values were calculated and summarized in Table 3. The corrosion rate, which is illustrated by i_{corr}, increases with the temperature. Commonly, the relation between the i_{corr} and temperature obeys the familiar Arrhennius equation: [19]

$$\frac{d(log i_{corr})}{d(\frac{1}{T})} = -\frac{E_a}{R} \qquad [10]$$

where E_a is the molar activation energy and R is the gas constant (8.314 J mol^{-1} K^{-1}). The Arrhenius plot is shown in Fig. 5. The activation energy of the anode corrosion process is calculated and equals to 14.6 kJ mol^{-1}. This low activation energy value (<40 kJ mol^{-1}) also indicates that the anode dissolution process is under diffusion control. [19,40]

Table 3. Corrosion parameters of the Cu-Zn-Ni alloy scraps in 45 g L^{-1} CuSO$_4$ solutions containing 160 g L^{-1} H$_2$SO$_4$ at different temperatures

Temp/°C	β_a/mV decade^{-1}	β_c/ mV decade^{-1}	i_{corr}/A	E_{corr}/V
25	117	147	1.554×10^{-3}	0.046
30	104	146	1.699×10^{-3}	0.062
40	130	170	2.804×10^{-3}	0.063
50	138	190	4.433×10^{-3}	0.071
60	149	199	5.955×10^{-3}	0.079
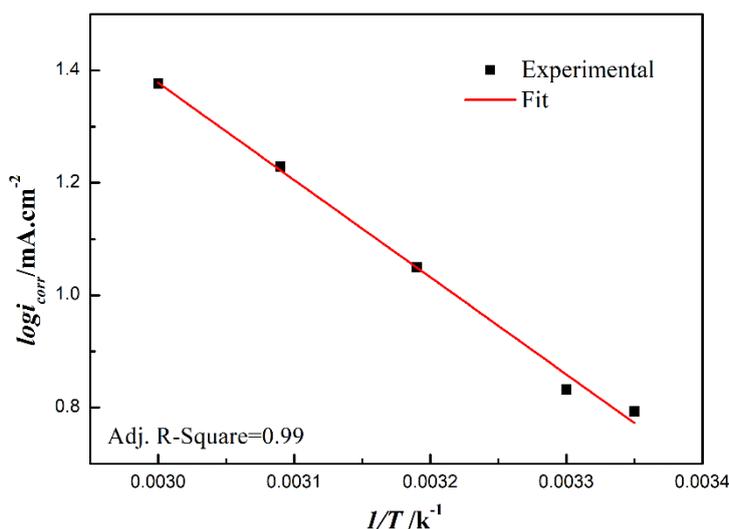
Figure 5. Arrhenius plot for Cu-Zn-Ni alloy scraps in 45 g L^{-1} CuSO$_4$ solutions containing 160 g L^{-1} H$_2$SO$_4$

3.3 Effect of heat treatment on the Cu-Zn-Ni alloy scraps anodic dissolution

Fig. 6 shows the microstructures of the Cu-Zn-Ni alloy scraps after treated in the as-cast, A and B conditions. It can be seen that there is no obvious precipitate to be found in these three samples. The microstructure of the as-cast condition (Fig. 6(a)) mainly consists of equiaxed grains and the size of the

grains is relatively small. However, after being treated in the A and B conditions, the size of the grains gradually increases and the particle size uniformity decreases, as seen from Fig. 6 (b) and (c). Further, the XRD results (Fig. 7) show that the main phase is all Cu_3ZnNi in these three samples, thereby indicating there is no new phase that formed after treated in conditions A and B.
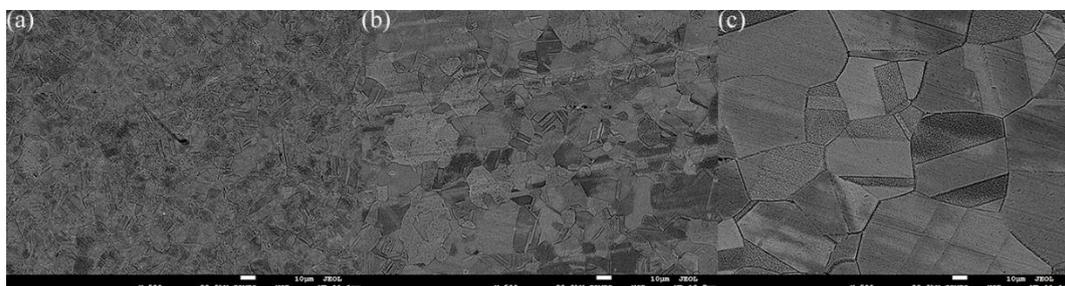
Figure 6. Microstructures of the Cu-Zn-Ni alloy scraps treated in conditions of as-cast, A and B
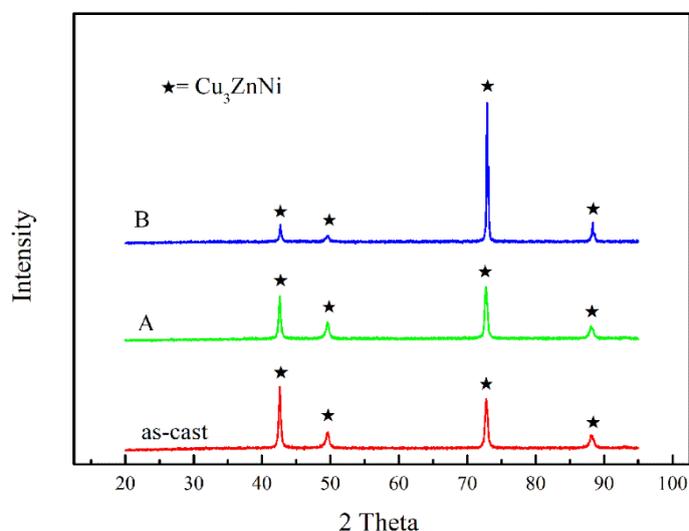
Figure 7. X-ray diffraction patterns of Cu-Zn-Ni alloy scraps treated in conditions of as-cast, A and B

The potentiodynamic polarization curves of the specimens after treated in conditions of as-cast, A and B are shown in Fig. 8. Table 4 lists the values of β_a, β_c, i_{corr} and E_{corr} for the tested alloy scraps in the above three conditions. Compared to those for the as-cast condition, the E_{corr} value decreases and i_{corr} value increases for the sample in the A condition. For the sample in the B condition, the measured E_{corr} value is more negative and the i_{corr} value is larger than those for the as-cast and A conditions. These indicate that the sample in the B condition is the most susceptible to dissolution. [28] Hence, it can be concluded that the anodic dissolution for the Cu-Zn-Ni alloy scraps is more susceptible when the size of the grains increases and the particle size uniformity decreases.
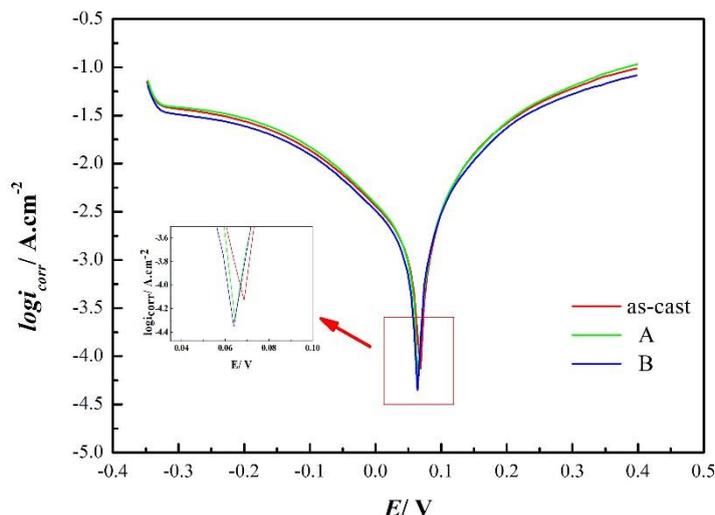
Figure 8. Potentiodynamic polarization curves for Cu-Zn-Ni alloy scraps treated in conditions of as-cast, A and B in 45 g L^{-1} CuSO$_4$ solutions containing 160 g L^{-1} H$_2$SO$_4$ at scan rate 5 mV s^{-1} and 25±1 °C

Table 4. Corrosion parameters of Cu-Zn-Ni alloy scraps treated in conditions of as-cast, A and B in 45 g L^{-1} CuSO$_4$ solutions containing 160 g L^{-1} H$_2$SO$_4$ at scan rate 5 mV s^{-1} at 25±1 °C

Heat treatment	β_a/mV decade^{-1}	β_c/mV decade^{-1}	i_{corr}/A	E_{corr}/V
As-cast	112	148	5.748×10^{-3}	0.050
A	119	148	6.549×10^{-3}	0.047
B	154	173	9.731×10^{-3}	0.043

Fig. 9 shows the Nyquist curves obtained at the Cu-Zn-Ni alloy scraps in the three above conditions at an open circuit potential. There are two capacitive loops in each Nyquist diagram under these three conditions. The charge transfer process leads the high-frequency capacitive loops, and the formation of corrosion products film leads to the low-frequency capacitive loops. [41, 42] It is noted that the Nyquist plot for the alloy scraps that are treated in the as-cast, A and B conditions are similar except for the loops diameters. This reveals that the dissolution mechanisms in these three conditions are similar, but the dissolution rates are different. The bigger capacitive loop indicates that the specimens' dissolution is more difficult. [43] Hence, the degree of dissolution which from easy to difficult in the three above conditions can be listed in the order that follows: B > A > as-cast. The result agrees with that of the polarization test.
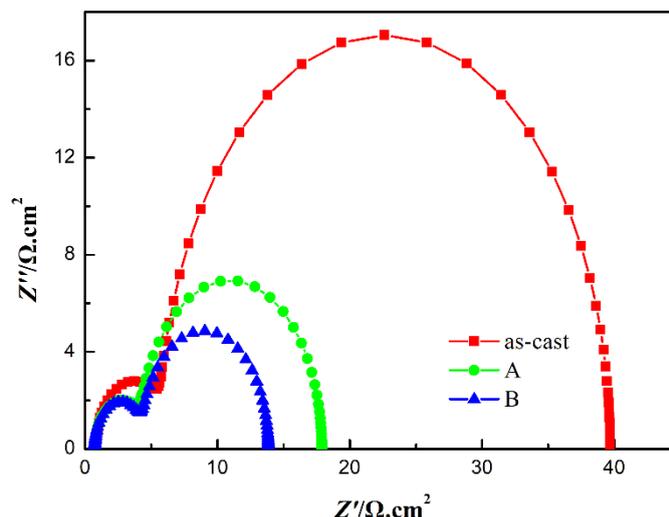
Figure 9. Nyquist plot for Cu-Zn-Ni alloy scraps treated in conditions of as-cast, A and B in 45 g L^{-1} CuSO$_4$ solutions containing 160 g L^{-1} H$_2$SO$_4$ at 25±1 °C

A simple equivalent circuit model (Fig. 10) was proposed to quantitatively describe the corrosion behavior of the Cu-Zn-Ni alloy scraps after treated in the as-cast, A and B conditions. In Fig. 10, R_s is the ohmic resistance of the test solution, R_{ct} represents the charge transfer resistance, C_{dl} is the double layer capacitance, R_{sf} represents the surface layer resistance, and C_{sf} is the surface layer capacitance. To obtain a better simulation between the equivalent circuit model and the experimental data, all elements were mathematically modeled using a constant phase element (CPE). The impedance is represented by the following mathematical formulation: [28]

$$Z_{(CPE)} = \frac{Z_0}{(j\omega)^n} \qquad [11]$$

where Z_0 is a constant, j is an imaginary number, ω is the angular frequency, and n is the correlation coefficient for the constant phase element, ranging 0-1.
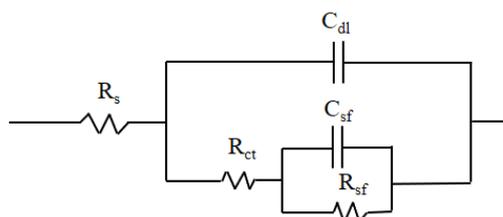
Figure 10. Equivalent circuit model used in the fitting of the impedance data

The calculated equivalent circuit parameters are presented in Table 5. The R_{ct} and R_{sf} for the A condition and B condition are lower than those for the as-cast condition. Namely, the resistance R_{sf} of the surface layer and the resistance R_{ct} of the charge transfer process decrease with the increase of the size of grains and the decrease of the particle size uniformity. The solution resistance R_s is affected little by the heat treatment, thereby reflecting the stability of the electrolyte.

Table 5. Impedance parameters for Cu-Zn-Ni alloy scraps treated in conditions of as-cast, A and B in 45 g L^{-1} CuSO$_4$ solutions containing 160 g L^{-1} H$_2$SO$_4$ at 25± 1 °C

Heat treatment	R_s Ω•cm^2	C_{dl} F•cm^2	R_{ct} Ω•cm^2	C_{sf} F•cm^2	R_{sf} Ω•cm^2
As-cast	0.84	4.15×10^{-6}	5.54	6.05×10^{-5}	33.30
A	0.74	3.39×10^{-6}	3.98	4.41×10^{-5}	13.18
B	0.73	5.75×10^{-6}	3.89	1.25×10^{-5}	9.23

4. CONCLUSION

We have shown from the electrochemical measurements and electron probe microscopic analysis how the sulfuric acid concentration, potential scan rate, temperature and heat treatment affect the anodic dissolution behavior of the Cu-Zn-Ni alloy scraps. The results show that with the H$_2$SO$_4$ concentration increasing from 0 to 160 g/L and the temperature increasing from 25 to 60 °C, the dissolution rate of the Cu-Zn-Ni alloy scraps increases. The anode peak current density that was derived from the cyclic polarization curves and the square root of the scan rate have a good linear correlation, and the activation energy of the anodic dissolution process is 14.6 kJ mol^{-1}, both of which indicate that the anodic dissolution process is under the control of diffusion. With the Cu-Zn-Ni alloy scraps that were first heat treated in proper conditions, the size of grains increases, and the particle size uniformity decreases, which results in the resistances of the surface layer and the charge transfer process decreasing and alloy scraps being more soluble.

References

1. J. Liu, S. Yang, W.S. Xia, X. Jiang and C.B. Gui, *J. Alloy. Compd.*, 654 (2016) 63
2. S. Gorsse, B. Ouvrard, M. Gouné and A. Poulon-Quintin, *J. Alloy. Compd.*, 633 (2015) 42
3. H. Nady, M. M. El-Rabiei, W.A. Badawy and M. Samy, *Journal of Bio- and Tribo-Corrosion*, 14 (2018) 2
4. I. Abacha and S. Boukhrissa, *Surf. Eng. Appl. Elect.*, 54 (2018) 459
5. A. Kaur, H.C. Boghani, E.M. Milner, R.L. Kimber, I.S. Michie, R. Daalmans, R.M. Dinsdale, A.J. Guwy, I.M. Head, J.R. Lloyd, E.H. Yu, J. Sadhukhan and G.C. Premie: *J. Hazard. Mater.*, 371 (2019) 18
6. D.A. Singer, *Ore Geol. Rev.*, 86 (2017) 271
7. J.F. Tang, M.H. Su, H.G. Zhang, T.F. Xiao, Y. Liu, Y.F. Liu, L.Z. Wei, C. Ekberg and B.M. Steenari, *Waste Manage.*, 76 (2018) 225
8. M. Ghodrat, M.A. Rhamdhani, G. Brooks, M. Rashidi and B. Samali, *Environ. Dev.*, 24 (2017) 36
9. Y.J. Ma and K.Q. Qiu, *Vacuum*, 106 (2014) 5
10. A. Tuncu, V. Stazi, A. Akcil, E.Y. Yazici and H. Deveci, *Miner. Eng.*, 25 (2012) 28
11. I.A. Popescu, T. Varga, A. Egedy, S. Fogarasi, T. Chován, Á.I. Lucaci and P. Ilea, *Comput. Chem.*

Eng., 83 (2015) 214
12. A. Agrawal and K.K. Sahu, *Resour. Conserv. Recy.*, 54 (2010) 401
13. F. Tesfaye, D. Lindberg, J. Hamuyuni, P. Taskinen and L. Hupa, *Miner. Eng.*, 111 (2017) 209
14. I. Bellemans, E.D. Wilde, N. Moelans and K Verbeken, *Adv. Colloid. Interface.*, 255 (2018) 47
15. A.A. Llamas, A.V. Delgado, A.V. Capilla, C.T. Cuadra, M. Hultgren, M. Peltomäki, A. Roine, M. Stelter and M.A. Reuter, *Miner. Eng.*, 131 (2019) 51
16. M. Kavousi, A. Sattari, E.K. Alamdari and D.H. Fatmehsari, *Metall. Mater. Trans. B*, 49 (2018) 1464
17. E. Rudnik, M. Pierzynka and P. Handzlik, *J. Mater. Cycles Waste*, 18 (2016) 318
18. E. Rudnik, K. Kołczyk and D. Kutyła, *Trans. Nonferrous Met. Soc. China*, 25 (2015) 2763
19. S. W. Qiu, L. Li, H. Wang and Y. Wang, *J. Electrochem. Soc.*, 164 (2017) 123
20. R. Gana, M. Figueroa, L. Kattan and S. Castro, *J Appl. Electrochem.*, 23 (1993) 813
21. M. Figueroa, R. Gana, L. Kattan, S.Me. Ndez and L. Palma, *J. Appl. Electrochem.*, 27 (1997) 99
22. F. Wang, H.J. Li and L. Li, *J. The Chinese Journal of Process Engineering.*, 16 (2016) 266
23. W.A. Badawy, R.M. El-Sherif and H. Shehata, *Electrochim. Acta*, 54 (2009) 4501
24. K.M. Ismail, R.M. Elsherif and W.A. Badawy, *Electrochim. Acta*, 49 (2004) 5151
25. M.A. Amin, S.A.E. Rehim and A.S. El-Lithy, *Electrochim. Acta*, 55 (2010) 5996
26. Y. Lu, A.R. Bradshaw, Y.L. Chiu and I.P. Jones, *Mat. Sci. Eng. C-Mater.*, 48 (2015) 480
27. Q.Q. Wu, G.L. Wei, G.H. Wu, W.C. Liu, T.P. Xuan and W. J. Ding, *China Foundry*, 13 (2016) 276
28. S.Y. Chen, K.H. Chen, G.S. Peng, L. Jia and P.X. Dong, *Mater. Design*, 35 (2012) 93
29. U. Tabrizi, R. Parvizi, A. Davoodi and M. H. Moayed, *Bull. Mater. Sci.*, 35 (2012) 89
30. T. Marlaud, A. Deschamps, F. Bley, W. Lefebvre and B. Baroux, *Electrochim. Acta*, 58 (2010) 248
31. M.H. Yen, J.H. Liu, J.M. Song and S.C. Lin, *J. Electron. Mater.*, 46 (2017) 5150
32. S.Y. Ji, S.H. Liang, K.X. Song and Q. Wang, *J. Wuhan. Univ. Technol.*, (2016) 408
33. L.P. Yu, Y. Jiang, Y.H. He and C.T. Liu, *J. Alloy. Compd.*, 638 (2015) 7
34. J. Oh, and C. V. Thompson, *Electrochim. Acta*, 56 (2011) 4044
35. A.M. Lafront, F. Safizadeh, E. Ghali and G. Houlachi, *Electrochim. Acta*, 55 (2010) 2505
36. X.D. Kong, H.E. hu and X.H. Su, *Introduction to Metal Corrosion and Protection, 1st ed.*, Science Press, BeiJing, (2016) 152
37. S.K.H. Darzi, *Chinese J. Catal.*, 39 (2018) 283
38. J.S. Li, L. Wang, W.S. You, M.Y. Liu, L.C. Zhang and X.J. Sang, *Chinese J. Catal.*, 39 (2018) 534
39. R.M. ElSherif, K.M. Ismail and W.A. Badawy, *Electrochim. Acta*, 49 (2004) 5139
40. D.W. Yang, Q.Y. Li, F.X. Shen, Q. Wang, L. Li, N. Song, Y.N. Dai and J. Shi, *Electrochim. Acta*, 189 (2016) 32
41. M. Menkuer and H. Ozkazanc, *Prog. Org. Coat.*, 130 (2019) 149
42. H. Nady, M.M. El-Rabiei and M. Samy, *J. Petrol. Sci. Eng.*, 26 (2017) 79